
BLIPs: Bayesian Learned Interatomic Potentials

Dario Coscia*
mathLab, SISSA
University of Amsterdam

Pim de Haan
CuspAI

Max Welling
CuspAI
University of Amsterdam

Abstract

Machine Learning Interatomic Potentials (MLIPs) are becoming a central tool in simulation-based chemistry. However, like most deep learning models, MLIPs struggle to make accurate predictions on out-of-distribution data or when trained in a data-scarce regime, both common scenarios in simulation-based chemistry. Moreover, MLIPs do not provide uncertainty estimates by construction, which are fundamental to guide active learning pipelines and to ensure the accuracy of simulation results compared to quantum calculations. To address this shortcoming, we propose BLIPs: Bayesian Learned Interatomic Potentials. BLIP is a scalable, architecture-agnostic variational Bayesian framework for training or fine-tuning MLIPs, built on an adaptive version of Variational Dropout. BLIP delivers well-calibrated uncertainty estimates and minimal computational overhead for energy and forces prediction at inference time, while integrating seamlessly with (equivariant) message-passing architectures. Empirical results on simulation-based computational chemistry tasks demonstrate improved predictive accuracy with respect to standard MLIPs, and trustworthy uncertainty estimates, especially in data-scarce or heavy out-of-distribution regimes. Moreover, fine-tuning pretrained MLIPs with BLIP yields consistent performance gains and calibrated uncertainties.

1 Introduction

Deep learning is transforming computational chemistry and materials science, enabling advances in molecular design (Özçelik et al., 2024; Eijkelboom et al., 2024; Zeni et al., 2023; Merchant et al., 2023), simulation-based modelling (Batatia et al., 2022; Wood et al., 2025; Neumann et al., 2024), and particle-based systems (Kipf et al., 2018; Alkin et al., 2024; Zhdanov et al., 2025). At the forefront of this progress are Message Passing Neural Networks (MPNNs) (Scarselli et al., 2008; Kipf and Welling, 2016; Gilmer et al., 2017), which have emerged as core architectures for learning in atomistic and molecular domains. Their ability to natively incorporate essential physical symmetries, such as translational, rotational, and permutation invariance or equivariance (Cohen and Welling, 2016; Weiler et al., 2023; Bronstein et al., 2017; Cohen et al., 2019), makes them particularly well-suited for modelling the complex interactions that define atomic-scale systems. Consequently, MPNNs are now widely adopted in the development of Machine Learning Interatomic Potentials (MLIPs), where they serve as efficient and accurate surrogates for quantum and classical simulations. These models enable large-scale atomistic simulations with near ab initio accuracy, dramatically accelerating research in materials discovery, catalysis, and molecular dynamics (Wood et al., 2025; Neumann et al., 2024; Batatia et al., 2022).

However, like most deep learning models, MLIPs are vulnerable to failure, particularly when faced with out-of-distribution (OOD) data. This issue is further worsened in scientific domains, where generating labelled data often requires expensive and time-consuming simulations (Papamarkou et al., 2024). Indeed, for simulation-based chemistry, training data is often obtained from Density

*Correspondence: dario.coscia@sissa.it

Functional Theory (DFT) calculations, which scale cubically with system size, making it impractical to generate data for larger molecules or materials. Moreover, the chemical space is vast and inherently undersampled, making distributional shifts inevitable (Özçelik et al., 2025; Tan et al., 2023). These challenges make principled Uncertainty Quantification (UQ) essential for enabling error-aware simulations or guiding active learning pipelines. Among existing approaches, Deep Ensembles (Lakshminarayanan et al., 2017) are commonly used for UQ in MLIPs and have shown strong empirical performance compared to other UQ methods (Tan et al., 2023). However, they require training and storing multiple models, making them computationally and memory-intensive, particularly in large-scale or high-throughput scientific workflows. Other simpler UQ methods, such as MC Dropout (Gal and Ghahramani, 2016) or mixture models, tend to be less memory-intensive but provide worse uncertainty estimates, and their predictive accuracy may degrade compared to standard deterministic models.

To overcome these limitations, we introduce *Bayesian Learned Interatomic Potentials (BLIPs)*, a general variational Bayesian method that is scalable, accurate, and provides principled, well-calibrated uncertainty estimates for MLIPs. BLIP can be applied both when training or fine-tuning pretrained machine learning interatomic potentials. It builds on an adaptive version of Variational Dropout (Kingma et al., 2015), where the MPNNs’ weights are stochastically perturbed depending on the network’s input data. BLIP does not depend on the chosen MPNN architecture and seamlessly integrates with a vast family of invariant and equivariant models. Importantly, our approach adds minimal computational overhead compared to deterministic models in both training and predictive inference, while providing well-calibrated uncertainties and improvement in predictive accuracy. We evaluate our approach on various simulation-based chemistry tasks, focusing on small and large-scale systems. In both domains, we show that training with BLIP not only improves predictive performance but also produces meaningful uncertainty estimates. Furthermore, we demonstrate that fine-tuning a single pretrained MLIP with BLIP not only consistently improves predictive performance but also outperforms an ensemble of fine-tuned models, while simultaneously providing reliable uncertainty estimates. The code accompanying this work is available at <https://github.com/dario-coscia/blip>.

2 Background and Related Work

In this section, we present the relevant background on message passing neural networks, Bayesian modelling, uncertainty quantification, and machine learning force fields, which will later support the formulation of our proposed method.

2.1 Message Passing Neural Networks

Message Passing Neural Networks (Scarselli et al., 2008; Kipf and Welling, 2016; Gilmer et al., 2017) are a class of (permutation equivariant) neural networks that process graph-structured data. Given a Graph $\mathcal{G} = (\mathcal{V}, \mathcal{E})$ with nodes $v_i \in \mathcal{V}$, and edges $e_{ij} \in \mathcal{E}$, the MPNNs operations for each layer $l = 0, \dots, L - 1$ can be summarised as:

$$\begin{aligned} \text{message + aggregation: } \mathbf{m}_i^{l+1} &= \bigoplus_{j \in \mathcal{N}(i)} M_l(\mathbf{h}_j^l, a_{ij}) \\ \text{update: } \mathbf{h}_i^{l+1} &= U_l(\mathbf{h}_i^l, \mathbf{m}_i^{l+1}) \end{aligned} \tag{1}$$

where \mathbf{h}_i^l is the feature vector for node i at layer l , a_{ij} are the edge attributes, and $\bigoplus_{j \in \mathcal{N}(i)}$ is a permutation invariant pooling operation over the node i neighbors $\mathcal{N}(i)$ (e.g. sum or mean). Finally, M_l, U_l are learnable message and update functions usually approximated with small neural networks.

2.2 Bayesian Models and Uncertainty Quantification

Bayesian models have a long history in Deep Learning (Hinton and Van Camp, 1993; Welling and Teh, 2011; Graves, 2011; Blundell et al., 2015; Gal and Ghahramani, 2016), providing a principled framework for modelling uncertainty through probabilistic inference. Instead of treating neural network weights as fixed parameters, Bayesian approaches represent them as probability distributions, $\omega \sim p(\omega)$. Given a dataset $\mathcal{D} = \{(\mathbf{x}_i, \mathbf{y}_i)\}_{i=1}^N$ of N i.i.d. input-output observations, the goal is to

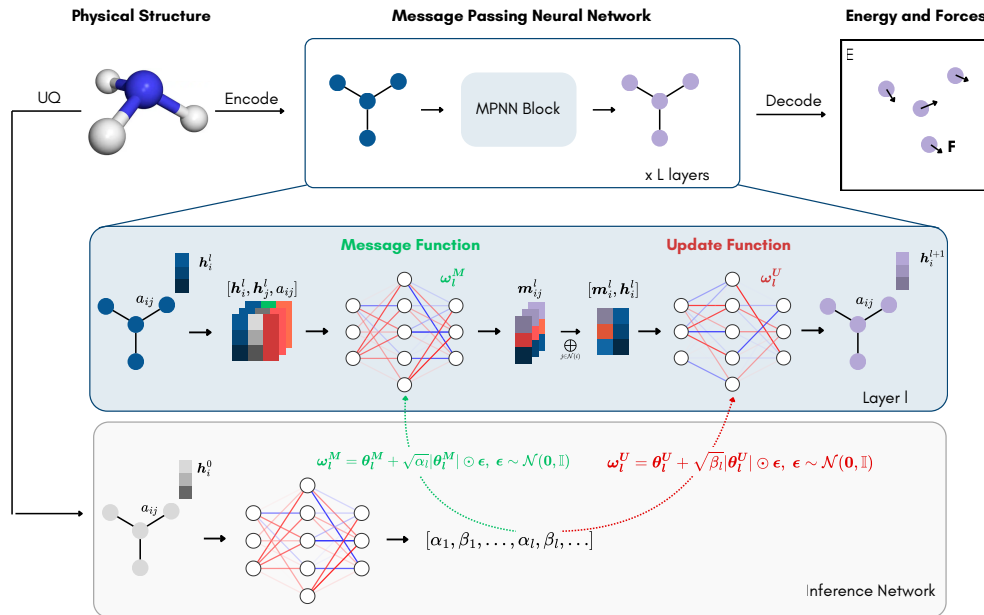


Figure 1: Bayesian Learned Interatomic Potentials (BLIPs) for Prediction and Uncertainty Quantification. An atomic structure is encoded as a graph, with initial node features h^0 and edge features a_{ij} , and processed by a standard Message Passing Neural Network (MPNN). BLIP introduces stochasticity into the machine learned interatomic potential (MLIP) by injecting zero-mean Gaussian noise into the message and update functions. Specifically, the deterministic weights θ_l^M and θ_l^U are perturbed using perturbation scales α_l and β_l (obtained through an inference network), respectively, yielding stochastic weights ω_l^M and ω_l^U . The main weights θ_l^M and θ_l^U , and the inference network weights are trained jointly using variational inference. This transforms MLIP into BLIP, a probabilistic model, enabling principled uncertainty quantification and improved predictive accuracy.

infer the posterior distribution over weights, $p(\omega | \mathcal{D})$, using Bayes' theorem (Bayes, 1763). Predictive inference is then performed via Bayesian model averaging, where the predictive distribution is given by $p(\mathbf{y} | \mathbf{x}) = \mathbb{E}_{p(\omega | \mathcal{D})}[p(\mathbf{y} | \mathbf{x}, \omega)]$. However, due to the high dimensionality of weight spaces in modern deep networks, exact Bayesian inference is computationally intractable, necessitating approximate methods. Among these, *Deep Ensembles* approximate the posterior by training multiple networks with different random initialisations and aggregating their predictions (Lakshminarayanan et al., 2017) and has been shown to provide state-of-the-art results in many applications (Fort et al., 2019; Tan et al., 2023). Other widely used approaches include *Variational Inference* (Blundell et al., 2015; Kingma et al., 2015), which approximates the posterior with a tractable parametric distribution optimised via the evidence lower bound (ELBO), and *Monte Carlo Dropout*, which interprets dropout at test time as Bayesian inference (Gal and Ghahramani, 2016).

2.3 Machine Learning Interatomic Potentials

Density Functional Theory (DFT) (Hohenberg and Kohn, 1964; Kohn and Sham, 1965; Parr, 1989) is a widely used quantum mechanical method for calculating a range of properties for various atomic systems. Under the Born-Oppenheimer approximation (Born and Heisenberg, 1985) of DFT, the potential energy surface (PES) E of an atomic system can be computed as a function of positions \mathbf{r} and atomic numbers \mathbf{Z} . Forces can be obtained by taking the negative gradient with respect to atom positions, $\mathbf{F} = -\nabla_{\mathbf{r}} E(\mathbf{r}, \mathbf{Z})$. DFT calculations are computationally expensive, due to their cubic scaling with respect to the number of electrons, and to overcome this limitation, Machine Learning Interatomic Potentials (MLIPs) have emerged as efficient surrogates for it, aiming to approximate the PES accurately and their corresponding forces, using machine learning models. Among the broad family of machine learning models, (equivariant) MPNNs (Batatia et al., 2022; Fu et al., 2025; Neumann et al., 2024; Rhodes et al., 2025; Schütt et al., 2017) have shown remarkable success,

particularly due to their favourable linear scaling with system size and their ability to generalise across diverse chemical domains (Wood et al., 2025), including materials, catalysts, and molecular systems. In MPNNs-based MLIPs, atomic numbers \mathbf{Z} are usually encoded for building node features, while positions \mathbf{r} are used to process geometric information. Despite achieving high accuracy in predicting PES across a variety of atomic configurations, MLIPs often fail to generalise to out-of-distribution (OOD) data, yielding unreliable energy predictions when presented with atomic environments that differ significantly from those seen during training, e.g. out-of-equilibrium structures, or rare chemical compositions. However, only a few works have addressed UQ in MLIPs. Notably, Tan et al. (2023) demonstrated that Deep Ensembles remain the most effective across a variety of UQ methods, both in terms of predictive accuracy and uncertainty estimation. Despite their performance, Deep Ensembles suffer from poor efficiency, with training and inference costs scaling linearly with the number of ensemble members. Moreover, for large-scale foundation models, constructing and maintaining an ensemble is often infeasible due to the high computational and storage requirements, meaning that only a single pretrained model may be available for downstream tasks.

3 Methods

BLIP is a practical and easy-to-use approach for training or fine-tuning any MLIP using variational Bayesian inference. It treats the weights of the message and update functions stochastically by injecting input-dependent Gaussian noise, allowing the model to capture uncertainty that varies with the atomic input structure. In the next section, we describe how BLIP can be seamlessly integrated into standard MLIP architectures, trained across diverse tasks, and scaled to support large models.

3.1 Building Bayesian Interatomic Potentials

As previously mentioned, MLIPs are typically implemented using MPNNs, where both the message and update functions are parameterised by separate neural networks. Following the Bayesian paradigm, we model the message and update functions M_l and U_l at each layer l as Bayesian neural networks. Specifically, these functions are parameterized by random weights ω_i^M and ω_i^U , drawn independently from prior distributions, i.e., $p(\omega_i^M, \omega_i^U) = p(\omega_i^M)p(\omega_i^U)$. This formulation enables the message passing process to incorporate uncertainty in the parameters of both the message and update functions, allowing uncertainty to propagate across layers.

Assuming a complete factorisation across layers, the generative model for the hidden state \mathbf{h}_i^{l+1} at layer $l + 1$ is given by:

$$p(\mathbf{h}_i^{l+1}, \mathbf{h}_i^l, \omega_i^M, \omega_i^U) = p(\mathbf{h}_i^{l+1} | \mathbf{h}_i^l, \omega_i^M, \omega_i^U) p(\omega_i^M) p(\omega_i^U), \quad (2)$$

where the conditional distribution $p(\mathbf{h}_i^{l+1} | \mathbf{h}_i^l, \omega_i^M, \omega_i^U)$ is the pushforward induced by the standard message passing procedure:

$$\begin{aligned} \mathbf{m}_i^{l+1} &= \bigoplus_{j \in \mathcal{N}(i)} M_l(\mathbf{h}_j^l, a_{ij}; \omega_i^M) \\ \mathbf{h}_i^{l+1} &= U_l(\mathbf{h}_i^l, \mathbf{m}_i^{l+1}; \omega_i^U) \end{aligned} \quad (3)$$

which is a deterministic delta distribution, i.e. $p(\mathbf{h}_i^{l+1} | \mathbf{h}_i^l, \omega_i^M, \omega_i^U) = \delta(\mathbf{h}_i^{l+1} - g(\mathbf{h}_i^l; \omega_i^M, \omega_i^U))$ with g the function obtain with the message and update composition above. In practice, the model works by first sampling random weights for the message and update functions at each layer. Then, using these sampled weights, it performs the usual message-passing updates starting from the initial hidden state. The final output \mathbf{y} comes from the last layer’s hidden state \mathbf{h}^L , which depends on the initial features, edge attributes, and all sampled weights up to that layer. In other words, $\mathbf{h}^L = f(\mathbf{h}^0, a_{ij}, \{\omega_i^M, \omega_i^U\}_{l=0}^{L-1})$.

3.2 Variational Adaptive Dropout

Variational Posterior: To train the model, we introduce a variational posterior distribution over the weights, conditioned on the input features (initial node representations \mathbf{h}^0 and edge attributes a_{ij}). This allows the model to capture input-dependent uncertainty more accurately. Formally, we factorise the posterior as:

$$q_\phi(\omega_i^M, \omega_i^U | \mathbf{h}^0, a_{ij}) = q_\phi(\omega_i^M | \mathbf{h}^0, a_{ij}) q_\phi(\omega_i^U | \mathbf{h}^0), \quad (4)$$

where ϕ denotes the parameters of the approximate distribution. Following [Coscia et al. \(2025\)](#), we employ an efficient parameterisation based on Variational Dropout ([Kingma et al., 2015](#)), which enables scalable inference in large MPNN architectures thanks to the local-reparametrization trick ([Kingma et al., 2015](#)) (see Algorithm 1).

Specifically, in each message-passing layer l , the message and update functions can be parametrised by a multi-layer perceptron (MLP), which may consist of multiple successive linear layers. For example, the message function at layer l could be represented as an MLP with S linear layers. We model the weights of each such internal linear layer $s = 1, \dots, S$ using a Gaussian distribution²:

$$\begin{aligned} q_\phi(\omega_{ls}^M \mid \mathbf{h}^0, a_{ij}) &= \mathcal{N}(\theta_{ls}^M, \alpha_l(\theta_{ls}^M)^2), \\ q_\phi(\omega_{ls}^U \mid \mathbf{h}^0) &= \mathcal{N}(\theta_{ls}^U, \beta_l(\theta_{ls}^U)^2), \end{aligned} \quad (5)$$

where θ_{ls}^M and θ_{ls}^U are the mean weights of the message and update networks, respectively, and the squaring is applied element-wise. The *variational adaptive dropout* coefficients α_l and β_l are input-dependent:

$$\alpha_l = \alpha_l(\mathbf{h}^0, a_{ij}), \quad \beta_l = \beta_l(\mathbf{h}^0), \quad (6)$$

and are computed per edge and node, respectively.

This can be interpreted as injecting Gaussian noise into the weights, scaled by the corresponding variational dropout coefficients:

$$\begin{aligned} \omega_{ls}^M &= \theta_{ls}^M + \epsilon_{ls}^M \odot |\theta_{ls}^M|, \quad \epsilon_{ls}^M \sim \mathcal{N}(0, \alpha_l(\mathbf{h}^0, a_{ij})), \\ \omega_{ls}^U &= \theta_{ls}^U + \epsilon_{ls}^U \odot |\theta_{ls}^U|, \quad \epsilon_{ls}^U \sim \mathcal{N}(0, \beta_l(\mathbf{h}^0)), \end{aligned} \quad (7)$$

where \odot denotes element-wise multiplication. Due to the Gaussian assumption, the local reparameterization trick ([Kingma et al., 2015](#)) can be employed, allowing us to sample activations directly instead of weights. This drastically reduces the number of random samples per iteration, as we only need to sample once for every neuron activation rather than once for every weight, leading to both lower variance in the gradient estimates and improved computational efficiency (see Appendix D).

Encoding Variational Adaptive Dropout Coefficients The adaptive variance terms α_l and β_l are generated by a dedicated inference network E_ψ with two separate output heads. This inference network is shared across all layers l , meaning that the coefficients are computed once—based solely on the initial node features \mathbf{h}^0 and edge attributes a_{ij} , and then broadcast to each message-passing layer. As a result, the full set of trainable variational parameters ϕ consists of: (i) the unperturbed weights of the message-passing network, $\Theta = \{\theta_l^M, \theta_l^U\}_{l=0}^{L-1}$; and (ii) the inference network parameters ψ , which govern the input-dependent noise injected into each layer.

Evidence Lower Bound Optimisation We optimise the variational parameters ϕ by maximising the Evidence Lower Bound (ELBO), which trades off between data fit (the expected log-likelihood term) and model complexity (KL divergence between the posterior and the prior). The ELBO is given by:

$$\begin{aligned} \mathcal{L}(\phi) &= \mathbb{E}_{q_\phi}[\log p(\mathbf{y} \mid \mathbf{h}^0, a_{ij}, \{\omega_l^M, \omega_l^U\}_{l=0}^{L-1})] \\ &\quad - \sum_{l=0}^{L-1} (D_{\text{KL}}[q_\phi(\omega_l^M \mid \mathbf{h}^0, a_{ij}) \parallel p(\omega_l^M)] + D_{\text{KL}}[q_\phi(\omega_l^U \mid \mathbf{h}^0) \parallel p(\omega_l^U)]), \end{aligned} \quad (8)$$

where the expectation is taken over all stochastic weights $\{\omega_l^M, \omega_l^U\}_{l=0}^{L-1}$. In practice, we approximate the expectation using a single Monte Carlo sample from the variational posterior at each training iteration.

We adopt a zero-mean Gaussian prior with fixed layerwise variance, chosen to match the variance induced by dropout with probability $p \in [0, 1]$:

$$\begin{aligned} \omega_{ij;ls}^M &= \epsilon_{ij;ls}^M \cdot |\theta_{ij;ls}^M|, \quad \epsilon_{ij;ls}^M \sim \mathcal{N}\left(0, \frac{p}{1-p}\right), \\ \omega_{ij;ls}^U &= \epsilon_{ij;ls}^U \cdot |\theta_{ij;ls}^U|, \quad \epsilon_{ij;ls}^U \sim \mathcal{N}\left(0, \frac{p}{1-p}\right), \end{aligned} \quad (9)$$

²We assume the same number of internal layers for both message and update networks for notational simplicity, though the approach trivially generalises. We also factorise across this dimension.

for each message-passing layer l and internal linear layer s . This choice yields closed-form KL divergences for both terms in eq. (8), as reported in Appendix A.1. Algorithm 2 shows how to train MLIPs using BLIP.

3.3 Equivariance and Invariance Analysis

Many MLIP architectures are explicitly designed to be either *equivariant* or *invariant* to certain input transformations (Cohen and Welling, 2016; Weiler et al., 2023; Bronstein et al., 2017; Cohen et al., 2019). An *equivariant* network ensures that when the input is transformed (e.g., via translation or rotation), the output transforms accordingly. An *invariant* network is a special case of equivariant one, where it produces the same output regardless of such transformations. These properties are crucial when modelling atomic systems, where geometric symmetries should not alter the model’s predictions. BLIP can also be used in conjunction with *equivariant* or *invariant* MLIPs without violating their symmetry properties³. To ensure this, the variational dropout coefficients α and β must themselves be invariant, which can be achieved by implementing the inference network E_{ψ} as an invariant neural network. When α and β are invariant to input transformations, the local reparameterization trick can be safely applied to any equivariant networks whose learnable layers can be expressed as unconstrained linear transformations without an irreducible representation (irrep) dimension. This includes models such as those in (Satorras et al., 2021; Schütt et al., 2021; Köhler et al., 2019; Schütt et al., 2017). However, in its current form, it excludes other important classes of equivariant MLIPs, such as MACE (Batatia et al., 2022) and UMA (Wood et al., 2025), thereby motivating future work to bridge this gap.

4 Experiments

We demonstrate the effectiveness of BLIP across a range of simulation-based chemistry tasks. First, as an illustrative example, we use BLIP to model a controlled dynamical system of charged particles interacting via Coulomb forces in a bounded 3D space. We then apply BLIP to two challenging MLIP tasks: (i) training from scratch using the equivariant PaiNN architecture (Schütt et al., 2021) on a data-scarce, out-of-distribution ammonia (NH_3) system, and (ii) fine-tuning the pretrained ORB v3 model (Rhodes et al., 2025) on silica glass (SiO_2) with 699 atoms. In both cases, BLIP improves uncertainty calibration and predictive performance.

4.1 Charged Particle System

As an illustrative example, we begin by training BLIP to learn the dynamics of five charged particles confined in a three-dimensional box, where their interactions evolve according to Coulomb’s law. This setup serves as a simplified example to test the model’s ability to learn and perform uncertainty quantification in a simpler scenario than simulation-based chemistry.

Dataset and Metrics: We model a system composed of 5 particles, each carrying a positive or negative charge and associated with a position and velocity in 3D space. The dataset is provided by (Fuchs et al., 2020), and we use the same split for training and testing. The task is to predict the particle positions after 1000 timesteps, given their initial positions and velocities. We train the model using the standard mean squared error (MSE) loss, augmented with a KL divergence term for BLIP. We evaluate performance using three metrics: mean square error (MSE), negative log-likelihood (NLL), and the continuous ranked probability score (CRPS). Further dataset and metrics details are provided in Section B.

Implementation Details: We benchmark two architectures for this task: a standard Graph Neural Network (GNN) (Gilmer et al., 2017) and the Equivariant Graph Neural Network (EGNN) proposed by (Satorras et al., 2021) using the same network hyperparameters and training protocol as in (Satorras et al., 2021). For the GNN baseline, edge attributes are also encoded via a linear layer before being used in message passing, as we noticed a performance improvement. For each neural architecture,

³Although the model is equivariant in distribution, individual forward passes may break exact equivariance or invariance due to the injected noise. For a given input, different noise samples (which themselves do not need to be equivariant) can yield different outputs. However, when averaged across samples, the statistical moments remain equivariant.

Table 1: Future position mean square error (MSE) in the N-body system. Averages are computed over 4 random initialisation seeds.

Equivariant	Model	MSE $\times 10^{-1}$ (\downarrow)	NLL (\downarrow)	CRPS (\downarrow)
\times	GNN (base model)	$0.121^{\pm 0.004}$	-	-
	MC Dropout ($p = 0.2$)	$0.117^{\pm 0.001}$	$-7.83^{\pm 0.31}$	$0.043^{\pm 0.000}$
	MC Dropout ($p = 0.5$)	$0.138^{\pm 0.049}$	$-8.03^{\pm 2.13}$	$0.046^{\pm 0.011}$
	Deep Ensemble	$0.106^{\pm \text{NA}}$	$-3.89^{\pm \text{NA}}$	$0.034^{\pm \text{NA}}$
	BLIP (ours)	$0.092^{\pm 0.004}$	$-9.03^{\pm 0.50}$	$0.032^{\pm 0.001}$
\checkmark	EGNN (base model)	$0.069^{\pm 0.002}$	-	-
	MC Dropout ($p = 0.2$)	$0.099^{\pm 0.006}$	$-6.19^{\pm 0.42}$	$0.044^{\pm 0.006}$
	MC Dropout ($p = 0.5$)	$0.299^{\pm 0.011}$	$0.91^{\pm 0.26}$	$0.091^{\pm 0.001}$
	Deep Ensemble	$0.057^{\pm \text{NA}}$	$-16.22^{\pm \text{NA}}$	$0.020^{\pm \text{NA}}$
	BLIP (ours)	$0.060^{\pm 0.003}$	$-12.52^{\pm 0.72}$	$0.022^{\pm 0.001}$

we compare BLIP with different variants. First, we train the deterministic version of the models to establish a baseline for predictive accuracy. We then evaluate two Bayesian versions of the same architectures for UQ: Monte Carlo (MC) Dropout (Gal and Ghahramani, 2016), using different dropout probabilities; and Deep Ensembles (Lakshminarayanan et al., 2017) with four ensemble members. For BLIP, we employ an invariant inference network, using an MLP consisting of two linear layers of size 64 with swish activations, used for both the message and update coefficients. The MLP work directly on the invariant features without message-passing. The message inference network head takes as input the edge attribute a_{ij} together with \mathbf{h}_i^0 and \mathbf{h}_j^0 , whereas the update inference network head only takes \mathbf{h}^0 . Additional architecture and training details are provided in Section C.

Results: Table 1 reports the predictive performance and uncertainty quantification metrics on the particle system, averaged over four random seeds. Our method, BLIP, consistently outperforms MC Dropout at different dropout probabilities, and matches or exceeds Deep Ensembles in terms of both accuracy and uncertainty quality. In the non-equivariant setting (GNN), BLIP achieves the lowest MSE and best-calibrated uncertainty estimates, as indicated by the lowest NLL and CRPS. In the equivariant setting (EGNN), Deep Ensembles obtain the best overall performance, but only marginally surpass BLIP. Importantly, BLIP remains highly competitive while being significantly more efficient, requiring only a single model for both training and inference against four ensemble members for Deep Ensemble ($\times 4$ main model parameter size). Overall, these results demonstrate that BLIP offers high-quality uncertainty estimates without compromising predictive accuracy, and does so with lower computational overhead than common ensemble-based methods.

4.2 Learning Interatomic Potentials in Data-Scarce and Out-Of-Distribution Regimes

Machine Learning Interatomic Potentials (MLIPs) are surrogate models that approximate the potential energy surface (PES) of atomic systems. Once the PES is learned, atomic forces can be directly computed as the negative gradient of the energy with respect to atomic positions. Accurate MLIP models enable highly efficient atomic system simulations, paving the way for various applications, such as catalyst design, adsorbents for recycling CO_2 from the atmosphere, and efficient solar cells, among others. This experiment focuses on the study of the Ammonia (NH_3) molecule for assessing the model’s robustness to out-of-distribution (OOD) data. This is a common challenge in materials science, where training data may be biased toward equilibrium or near-equilibrium configurations.

Dataset and metrics: We use the Ammonia dataset introduced by (Tan et al., 2023), which consists of a small number of NH_3 molecular geometries sampled across a range of energy configurations. The training set includes 78 geometries corresponding to near-equilibrium configurations with energies in the range of 0 to 5 kcal/mol. The test set, in contrast, contains 129 out-of-distribution (OOD) geometries with energies spanning up to 70 kcal/mol, thereby evaluating model generalisation far from the training distribution. This setup enables us to assess both predictive accuracy and the reliability of uncertainty estimates in a realistic low-data, high-OOD regime. We evaluate performance using three

Table 2: Energy and Forces mean absolute error (MAE) in the Ammonia system. Averages are computed over 4 random initialisation seeds. Baseline models’ results are from Tan et al. (2023).

Model	MAE (\downarrow)	
	Energy [kcal/mol]	Forces [kcal/mol/Å]
Deep Ensemble	11.71	48.03
Evidential Regression	13.58	53.29
Mean Variance Estimate	13.47	53.56
Gaussian Mixture Model	12.51	50.17
BLIP (ours)	11.51 ± 0.75	41.93 ± 3.38

metrics: mean absolute error (MAE), expected calibration error (ECE), and the Spearman correlation. Further dataset and metrics details are provided in Section B.

Implementation Details: We adopt the (equivariant) PaiNN architecture (Schütt et al., 2021) as our machine learning interatomic potential. To ensure a fair comparison, we use the same hyperparameter settings, training protocol, and evaluation procedure as described in (Tan et al., 2023). We train the model by explicitly enforcing energy conservation, computing atomic forces as the negative gradient of the predicted potential energy with respect to atomic positions, and weighting the energy/forces terms accordingly to Tan et al. (2023). For BLIP, we employ a compact invariant posterior network consisting of two linear layers of size 64 with swish activations, used for both the message and update coefficients. The message inference network head takes as input the square norm of the positions $\|\mathbf{r}_i - \mathbf{r}_j\|^2$, whereas the update inference network head only takes an embedding of the element atomic number Z . Additional architecture and training details are provided in Section C.

Results: As shown in Table 2, BLIP achieves the best MAE performance across both energy and forces targets, outperforming all baseline models from (Tan et al., 2023). For energy prediction, BLIP achieves an MAE of 11.51 ± 0.75 , slightly better than the Deep Ensemble (11.71) and substantially better than other probabilistic methods. On force prediction, which is a more challenging task, BLIP shows a notable improvement with an MAE of 41.93 ± 3.38 , significantly lower than both the Deep Ensemble and other baselines. These results demonstrate that training an MLIP with BLIP yields superior predictive accuracy on both energy and force targets, without modifying the base architecture or requiring multiple models, as is the case with Deep Ensembles.

Regarding uncertainty estimation, Table 3 reports the expected calibration error (ECE) for the different models. ECE measures how well the estimated probabilities match the observed probabilities, which intuitively means that if a model predicts to be confident $n\%$ of the time, it should be correct approximately $n\%$ of the time. From the table, it is clear that BLIP is the most calibrated model, outperforming even the Deep Ensemble method. Additionally, we analyse the linear relationship between pre-

Table 3: Expected calibration error (ECE) for Forces [kcal/mol/Å] in the Ammonia system for OOD data. Averages are computed over 4 random initialisation seeds. Baseline models’ results are from Tan et al. (2023).

Model	ECE (\downarrow)
Deep Ensemble	0.108
Evidential Regression	0.120
Mean Variance Estimate	0.135
Gaussian Mixture Model	0.112
BLIP (ours)	0.091 ± 0.006

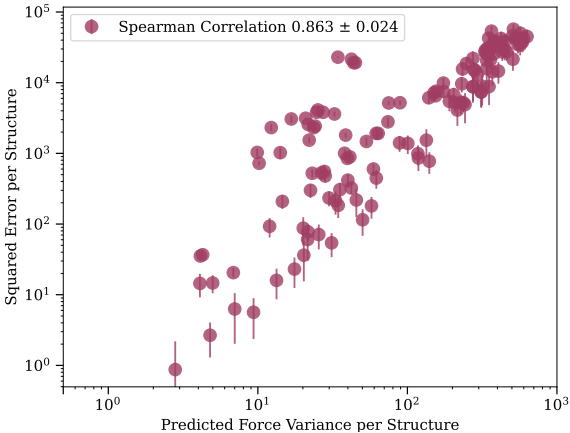


Figure 2: Spearman correlation between predicted uncertainty and squared mean error for Forces [kcal/mol/Å] in the Ammonia system for OOD data.

dicted uncertainty (variance) and squared error (Figure 2), which is particularly relevant for active learning. Our model demonstrates a strong linear correlation (Spearman correlation of 0.863 ± 0.024), indicating its reliability in identifying structures where the MLIP predictions are likely inaccurate.

4.3 Finetuning Pretrained Interatomic Potentials

The final set of experiments focuses on fine-tuning a pretrained MLIP. In the current era of increasing data and compute scale, training universal models from scratch is often impractical without large computational resources. Instead, it is common to fine-tune existing pretrained models. Among recent advancements, we select the ORB v3 Direct 200Mat model (Rhodes et al., 2025), a state-of-the-art direct force field that is not rotationally-equivariant. We fine-tune this model on a dataset composed of various silica (SiO_2) structures extracted from long and diverse molecular dynamics simulations. Each configuration contains 699 atoms in total, including 233 silicon and 466 oxygen atoms. This dataset presents a realistic and challenging benchmark, as the formation of large bulk structures makes DFT calculations computationally expensive.

Dataset and metrics: The silica glass (SiO_2) dataset introduced by (Tan et al., 2023) consists of system snapshots extracted from diverse, long molecular dynamics trajectories. These trajectories capture a range of physical conditions, including temperature equilibration, cooling, uniaxial tension, compression, and more (see Tan et al. (2023) for details on dataset generation). We fine-tune models using varying numbers of training samples (32, 128, and 1024) and evaluate performance on a held-out test set of 373 samples. Importantly, no structurally similar configurations appear in both the training and test sets, ensuring a robust evaluation. An example configuration from the dataset is shown in Figure 3a. This experimental setup allows us to assess both predictive accuracy under varying data regimes and the reliability of uncertainty estimates in a realistic application. We report performance using three metrics: mean absolute error (MAE), expected calibration error (ECE), and Spearman correlation. Further details on the dataset and evaluation metrics can be found in Section B.

Implementation details: We fine-tune the non-conservative ORB v3 model, originally trained on a subset of ab-initio molecular dynamics data from OMAT 24 (Barroso-Luque et al., 2024). We select ORB v3 due to its strong performance among state-of-the-art MLIPs and its low inference latency, benefiting from its non-conservative nature, which eliminates the need for automatic differentiation during force computation. All models are fine-tuned for 50 epochs using a batch size of 8, in float32-high precision, with the AdamW optimiser and cosine scheduler. The loss function minimises the Huber loss (as in Rhodes et al. (2025)) for both energy and force predictions. For BLIP, we employ a compact posterior network composed of four linear layers with hidden size 64 and swish activations for both the message and update functions. The edge network takes as input a concatenation of the pairwise distance vector (normalised to unit length) and 20 Gaussian radial basis functions applied to the raw edge distance. The node network processes atomic number embeddings. Finally, dropout probabilities p are predicted and transformed into multiplicative noise coefficients using the expression $p/(1-p)$. Additional architectural and training details are provided in Section C.

Results: Figure 3b shows the results of fine-tuning the ORB v3 model on the Silica dataset. For comparison, we include in the caption the best-performing model reported in the literature on this dataset, a Deep Ensemble Equivariant PaiNN (4 members) from (Tan et al., 2023). Notably, this model yields a substantially higher error than even the pretrained ORB v3 model (**pretrained**), highlighting the potential advantages of universal MLIPs. We then fine-tuned ORB v3 both with (**w/**) and without (**w/o**) BLIP. For inference with the BLIP fine-tuned models, we evaluated predicted forces using two approaches: (i) the sample mean computed from 100 stochastic forward passes (**sample mean**, Algorithm 3), and (ii) a single forward pass using the unperturbed weights (Gal and Ghahramani, 2016; Blundell et al., 2015), i.e., the maximum a posteriori estimate (**MAP estimate**, Algorithm 4). We also fine-tuned a Deep Ensemble of 4 members for direct comparison.

The results demonstrate that BLIP is both accurate and efficient. Using the sample mean or the more efficient MAP estimate, BLIP outperforms all ORB v3 baseline models and the pretrained PaiNN ensemble. Remarkably, BLIP with MAP inference achieves better accuracy than deepensembling the fine-tuned models, at a fraction of the computational cost, since it requires storing and fine-tuning only a single model. For uncertainty quantification, we evaluate ECE and Spearman correlation on the 1024-sample setup. BLIP achieves an ECE of 0.032 ± 0.002 , while Deep Ensemble performs

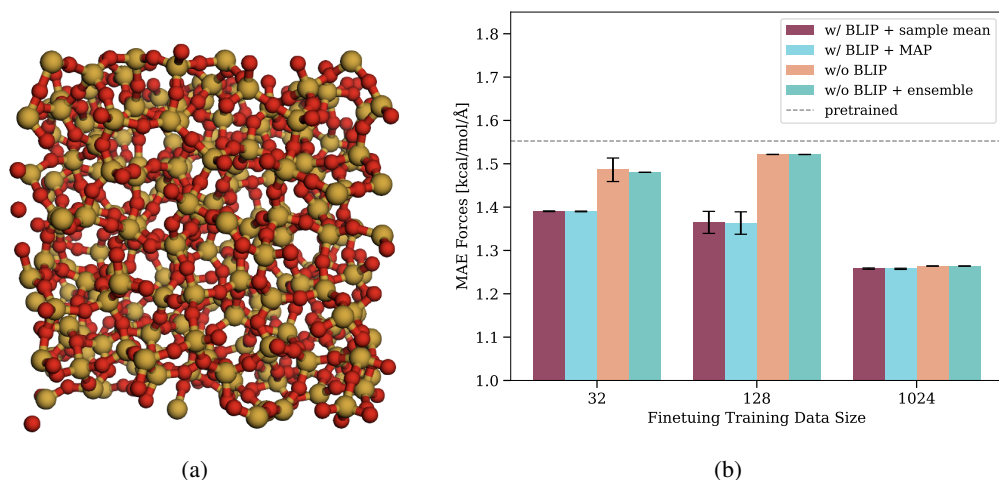


Figure 3: (a) Visualisation of the silica glass structure. (b) Forces mean absolute error (MAE) in the Silica system across different training sizes for finetuned ORB v3 direct 200MAT. Averages are computed over 4 random initialisation seeds, and the standard error of the mean is reported as an error bar. The best baseline model is a Deep Ensemble Equivariant PaiNN from [Tan et al. \(2023\)](#) trained on the 1024 configuration (same split), achieving MAE 6.58 kcal/mol/Å.

significantly worse with 0.247. When examining the correlation between predicted variance and squared error, crucial for active learning, BLIP slightly underperform, with a Spearman correlation of 0.602 ± 0.002 versus 0.676 for Deep Ensemble.

Overall, the results highlight that BLIP provides accurate calibration and reliable uncertainty estimates for guiding model refinement. More importantly, fine-tuning with BLIP achieves higher predictive accuracy than both deterministic and ensemble baselines, while maintaining the same inference cost as a standard deterministic model.

5 Conclusions

We introduced BLIP, a scalable and architecture-agnostic variational Bayesian framework for principled uncertainty quantification in (equivariant) message passing neural networks. Based on Adaptive Variational Dropout (AVD), BLIP can be used for both training from scratch and fine-tuning pre-trained MPNNs. Unlike deep ensembles, it maintains the same inference-time efficiency as standard deterministic models for predictive tasks, while enabling well-calibrated uncertainty estimates through stochastic sampling. We demonstrated the effectiveness of BLIP across a range of scientific tasks, including particle prediction and machine-learned interatomic potentials. BLIP achieves remarkable performance in prediction and uncertainty quantification for MLIPs when trained in data-scarce and OOD regimes. Notably, we showed that fine-tuning pretrained MLIPs with BLIP consistently enhances model performance, outperforming both deterministic and ensemble-based baselines. In addition, the uncertainty estimates produced by BLIP are well-calibrated and strongly correlated with model error, making them particularly useful for downstream applications such as active learning and error detection. These results highlight the potential of BLIP to serve as a drop-in tool for improving the performance of MLIPs, or more generally MPNNs, and provide them with useful uncertainty estimates at no additional computational cost.

Impact Statement

This paper presents work aimed at advancing the field of machine learning for atomistic modeling, with the potential to accelerate scientific discovery in chemistry and the biological sciences. As machine learning-based atomistic modeling continues to evolve, we recognize that there are numerous potential societal consequences of this work. While we do not feel that any specific issues need to be highlighted, we emphasize the importance of ongoing discussions on ethical considerations and

best practices to ensure these technologies are developed and applied in ways that benefit society as a whole.

Acknowledgement

D. Coscia acknowledges the support provided by PRIN "FaReX - Full and Reduced order modelling of coupled systems: focus on non-matching methods and automatic learning" project. We acknowledge ISCRA for awarding this project access to the LEONARDO supercomputer, owned by the EuroHPC Joint Undertaking, hosted by CINECA (Italy). D. Coscia conducted the project when visiting the University of Amsterdam.

References

- Alemi, A., Poole, B., Fischer, I., Dillon, J., Saurous, R. A., and Murphy, K. (2018). Fixing a Broken ELBO. In *International conference on machine learning*, pages 159–168. PMLR.
- Alkin, B., Fürst, A., Schmid, S., Gruber, L., Holzleitner, M., and Brandstetter, J. (2024). Universal Physics Transformers: A Framework for Efficiently Scaling Neural Operators. *Advances in Neural Information Processing Systems*, 37:25152–25194.
- Barroso-Luque, L., Shuaibi, M., Fu, X., Wood, B. M., Dzamba, M., Gao, M., Rizvi, A., Zitnick, C. L., and Ulissi, Z. W. (2024). Open Materials 2024 (OMat24) Inorganic Materials Dataset and Models. *arXiv preprint arXiv:2410.12771*.
- Batatia, I., Kovacs, D. P., Simm, G., Ortner, C., and Csányi, G. (2022). MACE: Higher Order Equivariant Message Passing Neural Networks for Fast and Accurate Force Fields. *Advances in neural information processing systems*, 35:11423–11436.
- Bayes, T. (1763). An Essay towards solving a Problem in the Doctrine of Chances. By the late Rev. Mr. Bayes, FRS communicated by Mr. Price, in a letter to John Canton, A.M.F.R.S. *Philosophical transactions of the Royal Society of London*.
- Blundell, C., Cornebise, J., Kavukcuoglu, K., and Wierstra, D. (2015). Weight Uncertainty in Neural Networks. In *International conference on machine learning*, pages 1613–1622. PMLR.
- Born, M. and Heisenberg, W. (1985). Zur quantentheorie der molekeln. In *Original Scientific Papers Wissenschaftliche Originalarbeiten*, pages 216–246. Springer.
- Bronstein, M. M., Bruna, J., LeCun, Y., Szlam, A., and Vandergheynst, P. (2017). Geometric deep learning: going beyond Euclidean data. *IEEE Signal Processing Magazine*, 34(4):18–42.
- Cohen, T. and Welling, M. (2016). Group Equivariant Convolutional Networks. In *International conference on machine learning*, pages 2990–2999. PMLR.
- Cohen, T. S., Geiger, M., and Weiler, M. (2019). A General Theory of Equivariant CNNs on Homogeneous Spaces. *Advances in neural information processing systems*, 32.
- Coscia, D., Welling, M., Demo, N., and Rozza, G. (2025). Barnn: A bayesian autoregressive and recurrent neural network. *arXiv preprint arXiv:2501.18665*.
- Eijkelboom, F., Bartosh, G., Naesseth, C. A., Welling, M., and van de Meent, J.-W. (2024). Variational Flow Matching for Graph Generation. *arXiv preprint arXiv:2406.04843*.
- Fort, S., Hu, H., and Lakshminarayanan, B. (2019). Deep ensembles: A Loss Landscape Perspective. *arXiv preprint arXiv:1912.02757*.
- Fu, X., Wood, B. M., Barroso-Luque, L., Levine, D. S., Gao, M., Dzamba, M., and Zitnick, C. L. (2025). Learning smooth and expressive interatomic potentials for physical property prediction. *arXiv preprint arXiv:2502.12147*.
- Fuchs, F., Worrall, D., Fischer, V., and Welling, M. (2020). SE(3)-Transformers: 3D Roto-Translation Equivariant Attention Networks. *Advances in neural information processing systems*, 33:1970–1981.

- Gal, Y. and Ghahramani, Z. (2016). Dropout as a Bayesian Approximation: Representing Model Uncertainty in Deep Learning. In *international conference on machine learning*, pages 1050–1059. PMLR.
- Gilmer, J., Schoenholz, S. S., Riley, P. F., Vinyals, O., and Dahl, G. E. (2017). Neural Message Passing for Quantum Chemistry. In *International conference on machine learning*, pages 1263–1272. Pmlr.
- Graves, A. (2011). Practical Variational Inference for Neural Networks. *Advances in Neural Information Processing Systems*, 24.
- Higgins, I., Matthey, L., Pal, A., Burgess, C., Glorot, X., Botvinick, M., Mohamed, S., and Lerchner, A. (2017). beta-VAE: Learning Basic Visual Concepts with a Constrained Variational Framework. In *International conference on learning representations*.
- Hinton, G. E. and Van Camp, D. (1993). Keeping the Neural Networks Simple by Minimizing the Description Length of the Weights. In *Conference on Computational Learning Theory*.
- Hohenberg, P. and Kohn, W. (1964). Inhomogeneous electron gas. *Physical review*, 136(3B):B864.
- Kingma, D. P. and Ba, J. (2014). Adam: A method for stochastic optimization. *arXiv preprint arXiv:1412.6980*.
- Kingma, D. P., Salimans, T., and Welling, M. (2015). Variational Dropout and the Local Reparameterization Trick. In *Advances in Neural Information Processing Systems*.
- Kipf, T., Fetaya, E., Wang, K.-C., Welling, M., and Zemel, R. (2018). Neural Relational Inference for Interacting Systems. In *International conference on machine learning*, pages 2688–2697. Pmlr.
- Kipf, T. N. and Welling, M. (2016). Semi-Supervised Classification with Graph Convolutional Networks. *arXiv preprint arXiv:1609.02907*.
- Köhler, J., Klein, L., and Noé, F. (2019). Equivariant Flows: sampling configurations for multi-body systems with symmetric energies. *arXiv preprint arXiv:1910.00753*.
- Kohn, W. and Sham, L. J. (1965). Self-consistent equations including exchange and correlation effects. *Physical review*, 140(4A):A1133.
- Lakshminarayanan, B., Pritzel, A., and Blundell, C. (2017). Simple and Scalable Predictive Uncertainty Estimation using Deep Ensembles. *Advances in neural information processing systems*, 30.
- Loshchilov, I. and Hutter, F. (2017). Decoupled Weight Decay Regularization. *arXiv preprint arXiv:1711.05101*.
- Merchant, A., Batzner, S., Schoenholz, S. S., Aykol, M., Cheon, G., and Cubuk, E. D. (2023). Scaling deep learning for materials discovery. *Nature*, 624(7990):80–85.
- Neumann, M., Gin, J., Rhodes, B., Bennett, S., Li, Z., Choubisa, H., Hussey, A., and Godwin, J. (2024). Orb: A fast, scalable neural network potential. *arXiv preprint arXiv:2410.22570*.
- Özçelik, R., Brinkmann, H., Criscuolo, E., and Grisoni, F. (2025). Generative Deep Learning for de Novo Drug Design A Chemical Space Odyssey. *Journal of Chemical Information and Modeling*.
- Özçelik, R., de Ruiter, S., Criscuolo, E., and Grisoni, F. (2024). Chemical Language Modeling with Structured State Space Sequence Models. *Nature Communications*, 15(1):6176.
- Papamarkou, T., Skoularidou, M., Palla, K., Aitchison, L., Arbel, J., Dunson, D., Filippone, M., Fortuin, V., Hennig, P., Hernández-Lobato, J. M., et al. (2024). Position: Bayesian Deep Learning is Needed in the Age of Large-Scale AI. In *International Conference on Machine Learning*.
- Parr, R. G. (1989). Density functional theory of atoms and molecules. In *Horizons of Quantum Chemistry: Proceedings of the Third International Congress of Quantum Chemistry Held at Kyoto, Japan, October 29-November 3, 1979*, pages 5–15. Springer.

- Rhodes, B., Vandenhaute, S., Šimkus, V., Gin, J., Godwin, J., Duignan, T., and Neumann, M. (2025). Orb-v3: atomistic simulation at scale. *arXiv preprint arXiv:2504.06231*.
- Satorras, V. G., Hooeboom, E., and Welling, M. (2021). E(n) Equivariant Graph Neural Networks. In *International conference on machine learning*, pages 9323–9332. PMLR.
- Scarselli, F., Gori, M., Tsoi, A. C., Hagenbuchner, M., and Monfardini, G. (2008). The Graph Neural Network Model. *IEEE transactions on neural networks*, 20(1):61–80.
- Schütt, K., Kindermans, P.-J., Saucedo Felix, H. E., Chmiela, S., Tkatchenko, A., and Müller, K.-R. (2017). Schnet: A continuous-filter convolutional neural network for modeling quantum interactions. *Advances in neural information processing systems*, 30.
- Schütt, K., Unke, O., and Gastegger, M. (2021). Equivariant message passing for the prediction of tensorial properties and molecular spectra. In *International conference on machine learning*, pages 9377–9388. PMLR.
- Tan, A. R., Urata, S., Goldman, S., Dietschreit, J. C., and Gómez-Bombarelli, R. (2023). Single-model uncertainty quantification in neural network potentials does not consistently outperform model ensembles. *npj Computational Materials*, 9(1):225.
- Virtanen, P., Gommers, R., Oliphant, T. E., Haberland, M., Reddy, T., Cournapeau, D., Burovski, E., Peterson, P., Weckesser, W., Bright, J., van der Walt, S. J., Brett, M., Wilson, J., Millman, K. J., Mayorov, N., Nelson, A. R. J., Jones, E., Kern, R., Larson, E., Carey, C. J., Polat, İ., Feng, Y., Moore, E. W., VanderPlas, J., Laxalde, D., Perktold, J., Cimrman, R., Henriksen, I., Quintero, E. A., Harris, C. R., Archibald, A. M., Ribeiro, A. H., Pedregosa, F., van Mulbregt, P., and SciPy 1.0 Contributors (2020). SciPy 1.0: Fundamental Algorithms for Scientific Computing in Python. *Nature Methods*, 17:261–272.
- Weiler, M., Forré, P., Verlinde, E., and Welling, M. (2023). Equivariant and Coordinate Independent Convolutional Networks. *A Gauge Field Theory of Neural Networks*, page 110.
- Welling, M. and Teh, Y. W. (2011). Bayesian Learning via Stochastic Gradient Langevin Dynamics. In *Proceedings of the 28th international conference on machine learning (ICML-11)*, pages 681–688.
- Wood, B. M., Dzamba, M., Fu, X., Gao, M., Shuaibi, M., Barroso-Luque, L., Abdelmaqsoud, K., Gharakhanyan, V., Kitchin, J. R., Levine, D. S., et al. (2025). UMA: A Family of Universal Models for Atoms. *arXiv preprint arXiv:2506.23971*.
- Zeni, C., Pinsler, R., Zügner, D., Fowler, A., Horton, M., Fu, X., Shysheya, S., Crabbé, J., Sun, L., Smith, J., et al. (2023). MatterGen: a generative model for inorganic materials design. *arXiv preprint arXiv:2312.03687*.
- Zhdanov, M., Welling, M., and van de Meent, J.-W. (2025). Erwin: A Tree-based Hierarchical Transformer for Large-scale Physical Systems. *arXiv preprint arXiv:2502.17019*.

SUPPLEMENTARY MATERIALS

TABLE OF CONTENTS

A Proofs and Derivations	15
A.1 KL-divergence proof	15
A.2 Predictive Distribution and Uncertainty Estimates	15
B Dataset and Metrics	15
B.1 NBody System	16
B.2 Ammonia and Silica Glass Systems	16
C Architectures and Training Details	17
C.1 NBody System	17
C.2 Ammonia Molecule System	18
C.3 Silica Glass System	18
D Algorithms	19

A Proofs and Derivations

This Appendix Section is devoted to the formal proofs introduced in the main text.

A.1 KL-divergence proof

We want to compute $D_{\text{KL}}^{\text{tot}} = D_{\text{KL}}[q_{\phi}(\boldsymbol{\omega}^M | \mathbf{h}^0, a_{ij}) \| p(\boldsymbol{\omega}^M)] + D_{\text{KL}}[q_{\phi}(\boldsymbol{\omega}^U | \mathbf{h}^0) \| p(\boldsymbol{\omega}^U)]$. Due to factorisation on the layers, the KL divergence reads:

$$D_{\text{KL}}^{\text{tot}} = \sum_{l=1}^L \sum_{s=1}^S [D_{\text{KL}}[q_{\phi}(\boldsymbol{\omega}_{ls}^M | \mathbf{h}^0, a_{ij}) \| p(\boldsymbol{\omega}_{ls}^M)] + D_{\text{KL}}[q_{\phi}(\boldsymbol{\omega}_{ls}^U | \mathbf{h}^0) \| p(\boldsymbol{\omega}_{ls}^U)]] \quad (10)$$

For the variational posterior and prior defined as in the main text:

$$\begin{aligned} q_{\phi}(\boldsymbol{\omega}_{ls}^M | \mathbf{h}^0, a_{ij}) &= \mathcal{N}(\boldsymbol{\theta}_{ls}^M, \alpha_l(\boldsymbol{\theta}_{ls}^M)^2), & p(\boldsymbol{\omega}_{ls}^M) &= \mathcal{N}\left(0, \frac{p}{1-p}(\boldsymbol{\theta}_{ls}^M)^2\right), \\ q_{\phi}(\boldsymbol{\omega}_{ls}^U | \mathbf{h}^0) &= \mathcal{N}(\boldsymbol{\theta}_{ls}^U, \beta_l(\boldsymbol{\theta}_{ls}^U)^2), & p(\boldsymbol{\omega}_{ls}^U) &= \mathcal{N}\left(0, \frac{p}{1-p}(\boldsymbol{\theta}_{ls}^U)^2\right), \end{aligned} \quad (11)$$

the marginal divergences are analytical:

$$\begin{aligned} D_{\text{KL}}[q_{\phi}(\boldsymbol{\omega}_{ls}^M | \mathbf{h}^0, a_{ij}) \| p(\boldsymbol{\omega}_{ls}^M)] &= \frac{(\alpha_l + 1)(1-p)}{p} + \log\left(\frac{p}{1-p}\right) - \log(\alpha_l) - 1, \\ D_{\text{KL}}[q_{\phi}(\boldsymbol{\omega}_{ls}^U | \mathbf{h}^0, a_{ij}) \| p(\boldsymbol{\omega}_{ls}^U)] &= \frac{(\beta_l + 1)(1-p)}{p} + \log\left(\frac{p}{1-p}\right) - \log(\beta_l) - 1. \end{aligned} \quad (12)$$

In practice, we weight the KL term by a factor λ as normally done for ELBO optimisation (Alemi et al., 2018; Higgins et al., 2017).

A.2 Predictive Distribution and Uncertainty Estimates

This subsection shows how to use BLIP for inference and uncertainty quantification. In the inference case, we are interested in regressing the output from the input by marginalising over the weights, while in UQ we aim to model epistemic (model weight uncertainty) and/or aleatory uncertainty (data’s inherent randomness).

Predictive Distribution The model *predictive distribution* $p(\mathbf{y} | \mathbf{h}^L = f(\mathbf{h}^0, a_{ij}, \{\boldsymbol{\omega}_l^M, \boldsymbol{\omega}_l^U\}))$ is obtained by marginalizing over the weights $\boldsymbol{\omega}$ sampled from the posterior distribution:

$$p(\mathbf{y} | \mathbf{h}^L) = \mathbb{E}_{q_{\phi}} [p(\mathbf{y} | \mathbf{h}^L = f(\mathbf{h}^0, a_{ij}, \{\boldsymbol{\omega}_l^M, \boldsymbol{\omega}_l^U\}))]. \quad (13)$$

In practice, this corresponds to performing multiple stochastic forward passes through the network and averaging the outputs, following the standard Monte Carlo approximation of predictive distributions (Gal and Ghahramani, 2016). Alternatively, a deterministic approximation can be used by evaluating the network at the posterior mean weights when uncertainty is not needed.

Uncertainty Estimates The predictive distribution allows for a clear variance decomposition using the law of total variance:

$$\sigma^2 = \underbrace{\sigma_{\boldsymbol{\omega}}^2(\mathbb{E}[\mathbf{y} | \mathbf{h}^L])}_{\text{epistemic uncertainty}} + \underbrace{\mathbb{E}_{\boldsymbol{\omega}}[\sigma^2(\mathbf{y} | \mathbf{h}^L)]}_{\text{aleatoric uncertainty}}, \quad (14)$$

with $\mathbb{E}[\mathbf{y} | \mathbf{h}^L]$, $\sigma^2(\mathbf{y} | \mathbf{h}^L)$ the mean and variance of the distribution $p(\mathbf{y} | \mathbf{h}^L)$ respectively.

B Dataset and Metrics

This Appendix Section is devoted to dataset and metrics introduced in the main text.

B.1 NBody System

Dataset Generation and Availability: We utilise the dataset introduced by Fuchs et al. (2020), which consists of simulations of five particles interacting in a three-dimensional box under Coulomb’s law. This dataset is publicly available at: https://github.com/FabianFuchsML/se3-transformer-public/tree/master/experiments/nbody/data_generation. Following the setup of Satorras et al. (2021), we generate the dataset using the parameters `-num-train 10000 -seed 43 -suffix small`. We follow the protocol of Satorras et al. (2021) and use 3000 samples each for training, validation, and testing, ensuring that there is no overlap between the splits.

Metrics: We adopt three different metrics for prediction and uncertainty estimation. For prediction, we compute the mean squared error (MSE) between the predicted (mean) positions $\hat{\mathbf{y}}$ and the true positions \mathbf{y} :

$$\text{MSE}(\hat{\mathbf{y}}, \mathbf{y}) = \frac{1}{3N} \sum_{i=1}^N \sum_{k=1}^3 (y_i^k - \hat{y}_i^k)^2, \quad (15)$$

where the index k denotes the spatial dimensions and i indexes the data points.

For uncertainty estimation, we consider the negative log-likelihood (NLL) and the continuous ranked probability score (CRPS). The NLL assumes a Gaussian predictive distribution with mean $\hat{\mathbf{y}}$ and variance σ^2 , and is computed as:

$$\text{NLL}(\hat{\mathbf{y}}, \mathbf{y}, \sigma^2) = \frac{1}{N} \sum_{i=1}^N \sum_{k=1}^3 \left[\frac{(y_i^k - \hat{y}_i^k)^2}{2\sigma_i^{k2}} + \frac{1}{2} \log(2\pi\sigma_i^{k2}) \right]. \quad (16)$$

The CRPS is a proper scoring rule, often used in forecasting scenarios, that compares the full predicted distribution with the observed outcome, thus it also measure calibration, and is defined as:

$$\text{CRPS}(\hat{\mathbf{y}}, \mathbf{y}, \sigma^2) = \frac{1}{N} \sum_{i=1}^N \sum_{k=1}^3 \text{CRPS}_{\mathcal{N}}(y_i^k; \hat{y}_i^k, \sigma_i^{k2}), \quad (17)$$

where $\text{CRPS}_{\mathcal{N}}$ denotes the closed-form CRPS for a univariate Gaussian distribution: To compute the CRPS for a univariate Gaussian predictive distribution with mean \hat{y} , variance σ^2 , and ground truth y , we use the following closed-form expression:

$$\text{CRPS}_{\mathcal{N}}(y; \hat{y}, \sigma^2) = \sigma \cdot \left(z(2\Phi(z) - 1) + 2\phi(z) - \frac{1}{\sqrt{\pi}} \right), \quad (18)$$

where $z = \frac{y - \hat{y}}{\sigma}$, $\phi(z)$ and $\Phi(z)$ are the standard normal probability density function and cumulative distribution function, respectively.

B.2 Ammonia and Silica Glass Systems

Dataset Generation and Availability: For the ammonia system, we utilize the dataset introduced by Tan et al. (2023), which comprises a small number of NH_3 molecular geometries sampled across a range of energy configurations. The dataset is publicly available at: <https://archive.materialscloud.org/records/tz6a0-hsb25>. We follow the same training/validation/test split protocol as Tan et al. (2023).

For the silica glass system, we also use the dataset from Tan et al. (2023), which consists of large SiO_2 structures extracted from diverse, long molecular dynamics trajectories. These trajectories span a range of physical conditions, including temperature equilibration, cooling, uniaxial tension, compression, and more. The dataset is publicly available at: <https://archive.materialscloud.org/records/tz6a0-hsb25>. We adopt the same validation/test split protocol as Tan et al. (2023), and vary the size of the training set (32, 128, and 1024 samples).

Additional details regarding the DFT calculations used to generate both datasets are provided in the Supplementary Information of Tan et al. (2023).

Table 4: Summary of main training-related hyperparameters for different experiments. These hyperparameters are shared among different models. Adam is the optimiser in [Kingma and Ba \(2014\)](#), while AdamW the one in [Loshchilov and Hutter \(2017\)](#).

Hyper-parameter	NBody	Ammonia	Silica
Optimization Epochs	10000	500	50
Batch Size	100	64	8
Optimiser	Adam	Adam	AdamW
Loss	MSE	MAE	HuberLoss(delta=0.01)
Maximum learning rate	$5e - 4$	$1e - 3$	$1e - 5$
Learning rate scheduling	Constant	ReduceLROnPlateau	Cosine with Warmup
Gradient Clip Norm Value	NA	NA	0.5
Warmup Iteration Phase	NA	NA	5%

Metrics: We follow the same experimental procedure as [Tan et al. \(2023\)](#): for prediction we compute the mean absolute error between predicted energy and forces \hat{E}, \hat{F} against true ones:

$$\begin{aligned} \text{MAE}(\hat{E}, E) &= \frac{1}{N} \sum_{i=1}^N \sum_{k=1}^3 |E_i - \hat{E}_i|, \\ \text{MAE}(\hat{F}, F) &= \frac{1}{3N} \sum_{i=1}^N \sum_{k=1}^3 |F_i^k - \hat{F}_i^k|. \end{aligned} \quad (19)$$

where the index k denotes the spatial dimensions and i indexes the data points.

To evaluate uncertainty, we compute the Expected Calibration Error (ECE) on forces, following the approach proposed by [Tan et al. \(2023\)](#). This choice is motivated by the fact that forces are more sensitive to overfitting and distributional shift, and thus provide a more informative measure of epistemic uncertainty than energy-based metrics. We estimate uncertainties using the mean force per structure, denoted by \bar{F}_i for structure i , which is obtained by averaging the per-atom forces and flattening across the spatial dimensions. The corresponding standard deviation, $\bar{\sigma}_i$, is computed as the square root of the average variance norm per atom, following the procedure in [Tan et al. \(2023\)](#). The ECE is then computed as:

$$\text{ECE} = \int_0^1 |p - p_{obs}| dp, \quad p_{obs} = \frac{1}{N} \sum_{i=1}^N \mathbb{I} \left\{ \bar{F}_i \leq \mathbb{Q}_p[\hat{\bar{F}}_i, \bar{\sigma}_i] \right\} \quad (20)$$

where \mathbb{Q} is the gaussian cumulative density function. The integral is computed by trapezoidal rule. We further evaluate the rank correlation between predicted variance $\bar{\sigma}_i^2$ and squared error norm per atom using the Spearman correlation coefficients using the Scipy ([Virtanen et al., 2020](#)) implementation.

C Architectures and Training Details

All our models have been trained on a single 64GB A-100 Nvidia GPU. We report in Table 4 the hyperparameters used across experiments shared among different models.

C.1 NBody System

We benchmark two architectures for this task: a standard Graph Neural Network (GNN) and the Equivariant Graph Neural Network (EGNN), as described in the main text. These two architectures are also used for the probabilistic baselines.

For the GNN baseline, each particle’s initial position and velocity are embedded through a linear layer to produce the initial node features \mathbf{h}^0 , which are passed to the first GNN layer. Edge attributes are derived from pairwise charge interactions, computed as $a_{ij} = c_i c_j$, and are likewise passed through a linear layer before being used in message passing. Both the message and update functions are implemented as a four-layer MLP of the form

$$64 \rightarrow \text{swish} \rightarrow 64 \rightarrow \text{swish} \rightarrow 64 \rightarrow \text{swish} \rightarrow 64.$$

To compute the final particle positions, we use a regression head consisting of a two-layer MLP:

$$64 \rightarrow \text{swish} \rightarrow 64 \rightarrow \text{swish} \rightarrow 3.$$

For the EGNN baseline, we employ the velocity variant from Satorras et al. (2021), where the initial velocity norm of each particle is mapped through a linear layer and included in the initial node features \mathbf{h}_i^0 . Particle charges are again encoded as edge attributes via the pairwise product $a_{ij} = c_i c_j$. The message and update functions have the same parameterisation as in the GNN model. Following Satorras et al. (2021), no regression head is used, as the network directly predicts particle positions.

Regarding the baseline methods, for MC Dropout we follow Gal and Ghahramani (2016) and apply dropout with varying probabilities after all linear layers of the message-passing network. For Deep Ensemble, we train the same architecture four times with different random initialisation seeds.

Finally, for BLIP, we employ a compact invariant posterior network consisting of two linear layers of size 64 with swish activations, used for both the message and update coefficients. Dropout probabilities p are predicted and converted to coefficients via $p/(1-p)$. The message inference network head takes as input the edge attribute a_{ij} together with \mathbf{h}_i^0 and \mathbf{h}_j^0 , whereas the update inference network head only takes \mathbf{h}^0 . For stability, we clamp the maximum dropout probability to 0.8. During training, we use a prior dropout probability of 0.5 and weight the regularisation term D_{KL} by $\lambda = 0.01$.

C.2 Ammonia Molecule System

We adopt the PaiNN architecture (Schütt et al., 2021) as our machine learning interatomic potential. To ensure a fair comparison, we use the same hyperparameter settings as in Tan et al. (2023), which are publicly available at: https://github.com/learningmatter-mit/UQ_singleNN.

For BLIP, we employ a compact invariant posterior network consisting of two linear layers of size 64 with swish activations, used for both the message and update coefficients:

$$64 \rightarrow \text{swish} \rightarrow 64 \rightarrow \text{swish} \rightarrow \text{head-dim}.$$

The message inference network head takes as input the squared interatomic distance $\|\mathbf{r}_i - \mathbf{r}_j\|^2$, whereas the update inference network head takes only an embedding of the element atomic number Z . Additional architecture and training details are provided in Section C. For stability, we clamp the maximum dropout probability to 0.8. During training, we use a prior dropout probability of 0.5 and weight the regularisation term D_{KL} by $\lambda = 10$.

C.3 Silica Glass System

We adopt the ORB v3 architecture (Rhodes et al., 2025) as our machine learning interatomic potential, pretrained on ab initio molecular dynamics data from OMAT 24 (Barroso-Luque et al., 2024). The Deep Ensemble variant finetunes four different models with different initialisation seeds.

For BLIP, we employ a compact posterior network composed of four linear layers with hidden size 64 and swish activations for both the message and update functions:

$$64 \rightarrow \text{swish} \rightarrow 64 \rightarrow \text{swish} \rightarrow 64 \rightarrow \text{swish} \rightarrow 64 \rightarrow \text{swish} \rightarrow \text{head-dim}.$$

The edge network takes as input a concatenation of the pairwise distance vector (normalised to unit length) and 20 Gaussian radial basis functions applied to the raw edge distance. The node network processes atomic number embeddings. Finally, dropout probabilities p are predicted and transformed into multiplicative noise coefficients using the expression $p/(1-p)$. For stability, we clamp p to the range $[0.00001, 0.1]$. During training, we use a prior dropout probability of 0.01 and weight the regularisation term D_{KL} by $\lambda = 0.001$. The lower clamp values, λ , and reduced prior dropout are chosen because we find that the original ORB model weights are highly sensitive to even minimal perturbations, likely because they were not trained with dropout or other weight-perturbation techniques. In addition, we use a different learning rate ($1e-4$) for the inference network to enable faster adaptation compared to the pretrained weights.

D Algorithms

This section reports the pseudocode algorithms for training and performing inference using a BLIP.

Local-reparametrization trick: The local-reparametrization trick (Kingma et al., 2015) was introduced to efficiently sample the predictive distribution of Bayesian linear layers. For a single linear layer with input \mathbf{h} and weight matrix $\omega \sim \mathcal{N}(\boldsymbol{\theta}, \alpha\boldsymbol{\theta}^2)$, the output \mathbf{z} also follows a normal distribution:

$$\mathbf{z} \sim \mathcal{N}(\boldsymbol{\gamma}, \text{diag}(\boldsymbol{\delta})), \quad (21)$$

where each output element z_j can be written as

$$z_j = \gamma_j + \sqrt{\delta_j}\epsilon_j, \quad \epsilon_j \sim \mathcal{N}(0, 1), \quad (22)$$

with

$$\gamma_j = \sum_i h_i \theta_{ij}, \quad \delta_j = \alpha \sum_i h_i^2 \theta_{ij}^2. \quad (23)$$

This shows that instead of sampling weights ω directly, one can sample the output \mathbf{z} by sampling from a Gaussian with analytically computed mean and variance, which reduces variance and computational cost. Below the algorithmic version.

Algorithm 1 Local reparameterization trick: Given a minibatch of activations \mathbf{h} and probabilistic Gaussian weights $\omega = \boldsymbol{\theta} + \alpha|\boldsymbol{\theta}|\boldsymbol{\epsilon}$, $\boldsymbol{\epsilon} \sim \mathcal{N}(\mathbf{0}, \mathbf{I})$, compute the output of a linear layer using the local reparameterization trick. For the first layer, \mathbf{h} corresponds to the state-input.

```

1:  $\mathbf{m} \leftarrow \text{matmul}(\mathbf{h}, \boldsymbol{\theta})$ 
2:  $\text{std} \leftarrow \alpha \cdot \sqrt{\text{matmul}(\mathbf{h} \odot \mathbf{h}, \boldsymbol{\theta} \odot \boldsymbol{\theta})}$ 
3:  $\text{eps} \sim \mathcal{N}(\mathbf{0}, \mathbf{I})$ 
4: return  $\mathbf{m} + \text{std} \odot \text{eps}$ 

```

In standard deep learning libraries, the above algorithm can be easily implemented by overriding the linear layer module. In our source code, we provide built-in wrappers that implement this functionality for convenience and ease of use.

Training with BLIPs: Algorithm 2 outlines the training procedure for Bayesian Learned Interatomic Potentials. Given a graph representing an atomic configuration with initial node features \mathbf{h}^0 and edge attributes a_{ij} , the inference network E_{ϕ} first produces variational adaptive dropout (VAD) coefficients $\boldsymbol{\alpha}, \boldsymbol{\beta}$ for each Bayesian linear layer. These parameters define the uncertainty-aware weight distributions used in the subsequent message passing steps. At each layer $l = 0, \dots, L - 1$, the node features \mathbf{h}^l are updated using a message passing function that incorporates stochastic sampling via the local reparameterization trick (see Algorithm 1). After the final layer, the atomic representations $\mathbf{h}^{1:L}$ are aggregated to predict the total energy E . If the potential field is conservative, forces \mathbf{F} are obtained by differentiating the energy; otherwise predicted directly from the final layer features \mathbf{h}^L . The loss combines mean absolute errors on energy and forces with the KL divergence regularizer.

Inference with BLIPs. Uncertainty quantification is performed via multiple stochastic forward passes through the model using Monte Carlo (MC) sampling. Importantly, the inference network is evaluated only once to extract the variational parameters $\boldsymbol{\alpha}, \boldsymbol{\beta}$, which are reused across MC samples. This amortization significantly reduces computational overhead. While more accurate moment-matching approximations could be used for the output distributions, we leave this for future work.

If only predictive means are needed and uncertainty estimates are not required, a single deterministic forward pass can be performed using the mean of the variational distributions (i.e., without stochastic sampling), effectively matching the performance speed of a standard MLIP.

Algorithm 2 Training Bayesian Learned Interatomic Potentials: Given a graph representing an atomic configuration with initial node features \mathbf{h}^0 and edge attributes a_{ij} , the model is trained by sampling Bayesian weights, performing stochastic message passing, and computing energies and forces. The loss combines mean absolute errors on energy and force predictions with a KL divergence regularizer depending only on the VAD coefficients.

```

1: while not converged do
2:    $\alpha, \beta \leftarrow E_{\psi}(\mathbf{h}^0, a_{ij})$  {Encode inputs to obtain VAD coefficients for all layers}
3:   for layer  $l = 0, \dots, L - 1$  do
4:      $\mathbf{h}^{l+1} \leftarrow \text{MessagePassing}(\mathbf{h}^l, a_{ij}, \alpha^l, \beta^l)$  {Stochastic message passing using Alg. 1}
5:   end for
6:   Compute energy  $E$  from  $\mathbf{h}^{1:L}$  by pooling
7:   if field is conservative then
8:      $\mathbf{F} \leftarrow -\nabla E$ 
9:   else
10:    Compute forces  $\mathbf{F}$  directly from  $\mathbf{h}^L$ 
11:   end if
12:    $\mathcal{L} \leftarrow \lambda_E \text{MAE}_E + \lambda_F \text{MAE}_F + \lambda D_{\text{KL}}(\alpha, \beta)$  {Loss includes MAEs and KL divergence term from Eq. (10)}
13: end while

```

Algorithm 3 BLIP Inference with Uncertainty Quantification

```

1:  $\alpha, \beta \leftarrow E_{\psi}(\mathbf{h}^0, a_{ij})$  {Encode inputs to obtain VAD coefficients once}
2: energies  $\leftarrow []$ , forces  $\leftarrow []$ 
3: for each MC sample  $s = 1, \dots, S$  do
4:    $\mathbf{h}^0 \leftarrow$  initial node features
5:   for layer  $l = 0, \dots, L - 1$  do
6:      $\mathbf{h}^{l+1} \leftarrow \text{MessagePassing}(\mathbf{h}^l, a_{ij}, \alpha^l, \beta^l)$  {Sample weights via local reparametrization (Alg. 1)}
7:   end for
8:   Compute energy  $E^{(s)}$  from  $\mathbf{h}^{1:L}$  by pooling
9:   if field is conservative then
10:     $\mathbf{F}^{(s)} \leftarrow -\nabla E^{(s)}$ 
11:   else
12:    Compute  $\mathbf{F}^{(s)}$  directly from  $\mathbf{h}^L$ 
13:   end if
14:   Append  $E^{(s)}$  to energies,  $\mathbf{F}^{(s)}$  to forces
15: end for
16: Compute mean and variance statistics over energies and forces

```

Algorithm 4 BLIP Inference with only mean Energy and Forces prediction

```

1: for layer  $l = 0, \dots, L - 1$  do
2:    $\mathbf{h}^{l+1} \leftarrow \text{MessagePassing}(\mathbf{h}^l, a_{ij}, \mathbf{0}, \mathbf{0})$  {Use mean weights, no perturbation}
3: end for
4: Compute energy  $E$  from  $\mathbf{h}^{1:L}$  by pooling
5: if field is conservative then
6:    $\mathbf{F} \leftarrow -\nabla E$ 
7: else
8:   Compute  $\mathbf{F}$  directly from  $\mathbf{h}^L$ 
9: end if

```
